Unactivated PKR Exists in an Open Conformation Capable of Binding Nucleotides†

Peter A. Lemaire,‡ Ingrid Tessmer,§ Ranyelle Craig,‡ Dorothy A. Erie,§ and James L. Cole*,‡,||

Department of Molecular and Cell Biology and National Analytical Ultracentrifugation Facility, University of Connecticut, Storrs, Connecticut 06269-3125, and Department of Chemistry and Curriculum in Materials and Applied Sciences, University of North Carolina, Chapel Hill, North Carolina 27599-3290

Received March 21, 2006; Revised Manuscript Received May 12, 2006

ABSTRACT: The dsRNA-activated protein kinase, PKR, plays a pivotal role in the cellular antiviral response. PKR contains an N-terminal dsRNA binding domain (dsRBD) and a C-terminal kinase domain. An autoinhibition model has been proposed in which latent PKR exists in a closed conformation where the substrate binding cleft of the kinase is blocked by the dsRBD. Binding to dsRNA activates the enzyme by inducing an open conformation and enhancing dimerization. We have tested this model by characterizing the affinity and kinetics of binding of a nucleotide substrate to PKR. The fluorescent nucleotide mant-AMPPNP binds to unactivated PKR with a K_d of ~30 μM, and the affinity is not strongly affected by autophosphorylation or binding to dsRNA. We observe biphasic binding kinetics in which the fast phase depends on ligand concentration but the slow phase is ligand-independent. The kinetic data fit to a two-step model of ligand binding followed by a slow conformation change. The kinetics are also not strongly affected by phosphorylation state or dsRNA binding. Thus, the equilibrium and kinetic data indicate that the substrate accessibility of the kinase is not modulated by PKR activation state as predicted by the autoinhibition model. In atomic force microscopy images, monomers of the latent protein are resolved with three separate regions linked by flexible, bridgelike structures. The resolution of the individual domains in the images supports a model in which unactivated PKR exists in an open conformation where the kinase domain is accessible and capable of binding substrate.

PKR is a soluble protein kinase which is activated by dsRNA[1] (*1*). PKR is constitutively expressed in most mammalian cell types, but it is induced by type 1 interferons and plays a central role in the innate immunity defense against viral infection (*2*). In addition, PKR has been implicated in a variety of cellular signal transduction pathways (*3*). PKR is a member of the family of protein kinases which phosphorylate eIF2α, resulting in a blockage of translational initiation (*4*). Production of dsRNA during viral infection leads to PKR activation and inhibition of protein synthesis and apoptosis (*5*). PKR contains an N-terminal double-stranded RNA binding domain (dsRBD) and a C-terminal kinase domain. The dsRBD consists of two tandem copies of a widely distributed double-stranded RNA binding motif (*6*). In a NMR structure of a PKR dsRBD construct, each of the dsRNA binding motifs adopts the canonical α*ββββ*α fold with an ~20-amino acid intervening region that is unstructured in the absence of dsRNA (*7*). The PKR kinase domain structure is typical of eukaryotic protein kinases with a substrate binding site lying at the interface of the N- and C-terminal lobes (*8*).

An autoinhibition model for PKR has been proposed in which dsRNA binding activates the enzyme by inducing a conformational change that relieves the latent enzyme of the inhibition that is mediated by interaction of the dsRBD with the kinase domain (*9*−*12*). Photoaffinity labeling of PKR with ATP derivatives requires either the presence of dsRNA (*13*, *14*) or prior autophosphorylation (*14*), suggesting that enzymatic activation is associated with increased accessibility of the nucleotide binding site. Deletion of a portion of the N-terminal region of PKR encompassing the dsRBD can produce a constitutively active kinase capable of autophosphorylation and phosphorylation of eIF2α in the absence of dsRNA (*12*, *15*−*18*). In the context of a dsRBD construct, NMR resonances associated with the second dsRNA binding motif are broadened or disappeared upon addition of exogenous kinase domain, suggesting that it directly contacts the catalytic domain (*10*). Intrinsic tryptophan fluorescence (*19*) and electrophoretic mobility shift assays (*20*) support the existence of a dsRNA-induced conformational change.

In addition to increasing the accessibility of the active site, dsRNA binding is believed to enhance dimerization of PKR, which in turn facilitates intermolecular autophosphorylation (*21*). PKR is expressed in a latent form, but upon binding dsRNA, it undergoes autophosphorylation at multiple serine and threonine residues (*22*−*26*) as well as tyrosines (*27*), producing an activated enzyme form. Following autophosphorylation, PKR is constitutively active and is capable of phosphorylating exogenous substrates such as eIF2α in the

† This work was supported by Grant AI-53615 from the National Institutes of Health (J.L.C.) and by the American Cancer Society and NIH Grant GM-54136 (D.A.E.).

* To whom correspondence should be addressed. Telephone: (860) 486-4333. E-mail: james.cole@uconn.edu.

‡ Department of Molecular and Cell Biology, University of Connecticut.

§ University of North Carolina.

|| National Analytical Ultracentrifugation Facility, University of Connecticut.

[1] Abbreviations: AFM, atomic force microscopy; AMPPNP, adenylyl imidodiphosphate; dsRBD, dsRNA binding domain; dsRNA, double-stranded RNA; mant, *N*-methylanthraniloyl; WT, wild type.

10.1021/bi060567d CCC: $33.50
Published on Web 07/06/2006

absence of dsRNA (*14*, *21*, *28*). PKR exists in a weak monomer−dimer equilibrium with a K_d of 500 μM, and dimer stability is enhanced by ~500-fold upon autophosphorylation (*29*). Autophosphorylation can be induced without dsRNA by incubation of the enzyme at high concentrations, suggesting a model in which dsRNA functions to bring PKR monomers into proximity in a manner that is analogous to the dimerization of free PKR (*29*).

The activity of protein kinases is often tightly regulated. Structural studies reveal that the conformation of the catalytic core is conserved among protein kinases in the active state; however, the kinase domain adopts a diverse range of inactive conformations (*30*−*32*). Many kinases, including PKR, are activated by phosphorylation within the activation loop, which may improve the access of nucleotide or peptide substrates or realign critical catalytic residues. Kinetic and equilibrium binding measurements of diverse protein kinases indicate that activation loop phosphorylation consistently enhances the phosphoryl transfer rate by 2−4 orders of magnitude, but the effects on nucleotide and peptide substrate binding affinities are highly variable (*33*). In the structure of a complex of the PKR kinase domain with eIF2α, threonine 446 in the activation loop is phosphorylated and interacts with helix αC to correctly position catalytic residues. Phosphorylation at threonine 446 also allosterically regulates eIF2α binding (*8*, *34*).

A quantitative molecular description of PKR activation requires correlation of functional assays of PKR activation with direct measurement of dsRNA binding and enzymatic dimerization. However, detailed kinetic analysis of autophosphorylation reactions is generally difficult, and in the case of PKR, the analysis is complicated by the presence of ~15 autophosphorylation sites. Thus, we have investigated PKR activation by monitoring the affinity and kinetics of nucleotide binding to PKR in latent and activated states. Somewhat surprisingly, we find that the affinity and kinetics are largely unaffected by autophosphorylation or binding to dsRNA. These data argue against models in which dsRNA binding activates PKR by opening up the substrate binding cleft.

MATERIALS AND METHODS

Reagents and Materials. WT unphosphorylated PKR and the catalytically inactive K296R mutant were expressed in *Escherichia coli* and purified as previously described (*29*). Protein concentrations were measured by absorbance using an $\epsilon_{280} = 4.33 \times 10^4$ M^{-1} cm^{-1}. At enzyme concentrations of >0.5 μM, PKR undergoes dsRNA-independent autophosphorylation upon addition of ATP (*29*). PKR was phosphorylated by incubation in phosphorylation buffer [20 mM HEPES, 50 mM KCl, 5 mM $MgCl_2$, 0.1 mM EDTA, and 1 mM DTT (pH 7.5)] with 5 mM ATP at a protein concentration of 10−15 μM. The dimeric phosphoenzyme was purified by gel filtration on Superdex-200. We have previously demonstrated that this procedure results in essentially complete phosphorylation of PKR (*29*).

All solutions were prepared using Nanopure (resistivity of at least 18.2 MΩ cm) water. Mant-ATP and mant-AMPNP were purchased from Molecular Probes; mant-dATP was from Jena Bioscience (Jena, Germany), and unlabeled nucleotides (ATP, ADP, and AMPPNP) were obtained from Sigma. Nucleotide concentrations were measured by absorption using an ϵ_{255} of 2.33×10^4 M^{-1} cm^{-1} for mant-nucleotides and an $\epsilon_{259} = 1.54 \times 10^4$ M^{-1} cm^{-1} for unlabeled nucleotides. The complementary 40-nucleotide RNA sequences shown below were purchased from Dharmacon, deprotected using the manufacturer's instructions, and stored in TE buffer at −80 °C.

```
TS40: 5′-GGA GAA CUU CAU GCC CUU CGG AUA AGG ACU CGU AUG UAC C-3′
BS40: 3′-CCU CUU GAA GUA CGG GAA GCC UAU UCC UGA GCA UAC AUG G-5′
```

The RNA sequences were annealed in AU 200-Mg^{2+} buffer [20 mM HEPES, 200 mM NaCl, 5 mM $MgCl_2$, 0.1 mM EDTA, and 0.1 mM TCEP (pH 7.5)] by heating them to 70 °C and cooling them slowly to room temperature. RNA concentrates were determined using an ϵ_{260} of 6.62×10^5 M^{-1} cm^{-1}, and PKR was mixed with dsRNA at a PKR:dsRNA molar ratio of 2.5.

Equilibrium Fluorescence Measurements. Fluorescence intensity and anisotropy data were collected with a Fluoro-Max-3 fluorimeter equipped with Glan-Thompson polarizers (Jobin Yvon Inc.). All measurements were performed at 20 °C with samples in AU 200-Mg^{2+} buffer using a 1 cm × 0.2 cm microcuvette. Titrations were recorded with sequential additions of either enzyme or ligand with 4 min between additions. Buffer blanks were subtracted from the measured intensities, and intensities were corrected for dilution. Typically, equilibrium binding of mant-nucleotides is assessed by fluorescence energy transfer from tryptophans to mant (*35*, *36*). However, energy transfer in PKR is relatively inefficient, and binding was characterized by monitoring the fluorescence intensity or emission anisotropy increase with direct excitation of the mant-nucleotide at 360 nm. The anisotropy is defined by

$$r = \frac{I_{||} - GI_{\perp}}{I_{||} + 2GI_{\perp}} \quad (1)$$

where $I_{||}$ and $I_{\perp}$ are the intensities with the emission polarizers in the parallel and perpendicular orientations, respectively, with the excitation polarizer in the vertical (parallel) orientation. The G factor corrects for the polarization bias of the gratings and is given by the ratio of the intensities ($I_{||}/I_{\perp}$) with the excitation polarizer in the perpendicular orientation. G was determined initially for each experiment and fixed in subsequent measurements. Buffer backgrounds were subtracted for each polarizer orientation.

Dissociation constants were measured using a fixed concentration of mant-nucleotide titrated with PKR (forward titration) or a fixed enzyme concentration with addition of mant-nucleotide (reverse titration). Both types of titrations were fit using a 1:1 binding model with a single equilibrium dissociation constant, K_d. Under conditions where the enzyme and ligand concentrations are comparable, the concentration of the enzyme−ligand complex ([EL]) is given by

$$[\mathrm{EL}] = \frac{K_d + [\mathrm{E}]_0 + [\mathrm{L}]_0}{2} - \frac{\sqrt{(K_d + [\mathrm{E}]_0 + [\mathrm{L}]_0)^2 - 4[\mathrm{E}]_0[\mathrm{L}]_0}}{2} \quad (2)$$

where $[E]_0$ and $[L]_0$ are the total concentrations of enzyme and ligand, respectively. Binding isotherms were analyzed

using nonlinear least-squares fitting with Igor Pro (Wavemetrics, Lake Oswego, OR). For models in which a 1:1 stoichiometry was assumed, $[E]_0$ was fixed at the true enzyme concentration. Alternatively, $[E]_0$ was treated as an adjustable parameter, and the stoichiometry (N) was calculated as the ratio of $[E]_0$ to the actual concentration of PKR. Fluorescence intensity data were analyzed using the following equation:

$$I = I_0 + \frac{[EL]}{[L]_0}\Delta I \quad (3)$$

where I is the fluorescence intensity (corrected for dilution), I_0 is the fluorescence intensity in the absence of PKR, and ΔI is the limiting fluorescence increase due to PKR binding. The intensity data were fit by treating I_0, ΔI, and K_d as adjustable parameters. For analysis of anisotropy titrations, the measured anisotropy is the average anisotropies of the free ligand and the ligand bound to enzyme, weighted by their concentrations and their relative fluorescence intensities:

$$\langle r \rangle = \frac{r_L[L] + r_{EL}[EL](I_{EL}/I_L)}{[L] + [EL](I_{EL}/I_L)} \quad (4)$$

where r_L is the anisotropy of the free ligand, r_{EL} is the anisotropy of the ligand in the EL complex, and I_{EL}/I_L is the fluorescence intensity ratio. I_{EL}/I_L was separately measured for binding of the mant-nucleotide to each form of PKR that was studied. The anisotropy data were fit by treating r_L, r_{EL}, and K_d as adjustable parameters.

Competitive anisotropy titrations were used to determine the affinities of unlabeled nucleotides using a fixed concentration of PKR and mant-nucleotide and variable concentrations of unlabeled nucleotide. Because of the relatively weak binding of nucleotides to PKR, it is not feasible to completely saturate the enzyme with mant-nucleotide, and the analysis of the competition titration requires solution of a cubic equation to obtain [EL]. The competitive anisotropy titrations were analyzed using the solution described in Appendix 2 of ref *36*, constraining the total concentrations of labeled and unlabeled nucleotides, K_d (dissociation constant of the mant-nucleotide), and I_{EL}/I_L while allowing r_L, r_{EL}, K_U (dissociation constant of the unlabeled nucleotide), and $[E]_0$ to float.

Stopped-Flow Kinetics Measurements. The kinetics of mant-nucleotide binding and dissociation were measured using an Applied Photophysics fluorescence stopped-flow instrument (model SX.18MV). Mant-ATP was employed because autophosphorylation is not a complication on the short time scale of these measurements. All measurements were performed in AU 200-Mg^{2+} buffer at 20 °C with excitation at 295 nm. Emission was measured using a 400 nm long-pass glass filter (Edmund Industrial Optics). For measurement of association kinetics, 2 μM enzyme was mixed at a 1:1 ratio with variable concentrations of mant-nucleotide. Data were collected using 1000 points over 10 s. Between 10 and 24 traces were averaged at each nucleotide concentration, and the data were fit to single- and multiple-exponential decay functions using KaleidaGraph (Synergy Software). The dissociation kinetics were measured by displacement of bound mant-nucleotide with a large excess of ATP. Enzyme (2 μM) was pre-equilibrated with 80 μM mant-ATP and then mixed at a 1:1 ratio with 4 mM ATP. Data were collected using 1000 points over 10 s, and the resulting kinetic traces were fit to single- and multiple-exponential decay functions. Kinetic simulations (*37*) and global data analysis (*38*) were performed using KinTekSim.

Atomic Force Microscopy. Images were obtained with a Nanoscope III DI atomic force microscope (AFM) (Veeco, Santa Barbara, CA) with 512 × 512 pixel resolution and a scan rate of 3 Hz, using an E-type scanner (15 μm × 15 μm maximum scan size). AFM tips employed were Nanosensors NCL cantilevers with spring constants between 40 and 55 N/m and nominal resonance frequencies of 182−199 kHz (Molecular Imaging, Phoenix, AZ). All images were plane fitted and third-order flattened using DI imaging software before analysis. Experiments were carried out in 20 mM HEPES (pH 7.8), 50 mM NaCl, and 5 mM $MgCl_2$. Buffer solutions were filtered prior to experiments using 0.02 μm filters (Anatop 25, Whatman, Maidstone, U.K.) and heated for 10 min to 65 °C. Protein solutions were incubated at ambient temperature for 20 and 50 min. Samples were diluted to 20 nM PKR for deposition, and 20 μL was then immediately applied to the surface of freshly cleaved mica and rinsed with water after 30 s. The surface was blotted, dried under nitrogen, and imaged immediately. Surface-bound conformations of proteins are fixed after removal of the surrounding buffer solution and do thus not further change during the experiment. Visual analysis of the topography of PKR molecules and protein−dsRNA complexes was carried out using DI imaging software (Veeco). Volume analysis of protein peaks in the AFM images was achieved using Image SXM 169-3x software (S. Barrett, University of Liverpool, Liverpool, U.K.), as previously described (*39*, *40*). Between 300 and 1000 molecules of PKR from AFM images went into the statistical analysis.

RESULTS

Fluorescence Changes of Mant-Nucleotides upon Binding to PKR. In equilibrium experiments, which employed WT PKR, the nonhydrolyzable ATP analogue mant-AMPPNP or unlabeled AMPPNP was used to avoid complications from PKR-catalyzed autophosphorylation reactions. In control experiments, we confirmed that both mant-AMPPNP and AMPPNP are not substrates for PKR (data not shown). We then examined changes in mant-nucleotide fluorescence upon binding to PKR. Upon direct excitation of the mant fluorophore at 360 nm, the fluorescence emission of mant-AMPPNP at 443 nm increased ~1.5-fold upon addition of a large molar excess of WT unphosphorylated PKR or inactive K296R mutant. This enhancement could be reversed by competing the mant-labeled nucleotide with excess unlabeled AMPPNP or ATP (results not shown). In contrast to previous reports, these data suggest that ATP is able to bind inactive PKR. Because the mant absorption band at 360 nm strongly overlaps with PKR tryptophan emission at 346 nm, we examined whether mant-nucleotide binding could be detected via fluorescence resonance energy transfer. As shown in Figure 1A, mant-ATP fluorescence emission is observed upon excitation at 295 nm, and there is an ~10% intensity increase upon addition of 1 μM PKR. The fluorescence increase is reversed by adding an excess of ATP, indicating that the enhancement is due to resonance energy transfer from the PKR tryptophans to the bound mant. Using the same concentrations of mant-nucleotide and PKR, upon

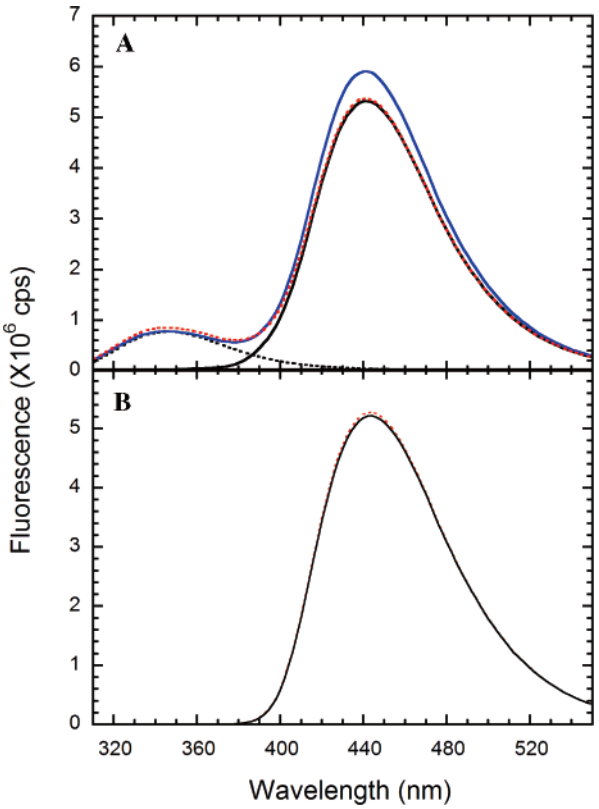

FIGURE 1: Fluorescence spectra of mant-ATP in the absence and presence of WT PKR: (A) mant-ATP (−), PKR (···), mant-ATP + PKR (blue trace) and mant-ATP + PKR + unlabeled ATP (red dotted trace). Spectra were recorded at an excitation wavelength of 295 nm with excitation and emission bandwidths of 2 nm. (B) Spectra of mant-ATP (−) and mant-ATP + PKR (red dotted trace). Spectra were recorded at an excitation wavelength of 360 nm with excitation and emission bandwidths of 2 nm. Concentrations were as follows: 122 μM mant-ATP, 1 μM PKR, and 2 mM ATP.

direct excitation of mant at 360 nm there is no increase in mant emission upon addition of PKR (Figure 1B), confirming that the observed enhancement in Figure 1A is due to fluorescence energy transfer. A greater extent of tryptophan → mant energy transfer is often observed upon binding of mant-nucleotides to ATP binding sites (e.g., refs *35* and *36*). Although PKR contains three tryptophans within the kinase domain, two of which are within ~15−20 Å of the ATP binding site, the mant moiety is perpendicular to the tryptophan indole rings in a model of mant-ATP bound to PKR, which is unfavorable for energy transfer (R. Brown and P. A. Lemaire, unpublished observations). Finally, we examined changes in mant-nucleotide emission anisotropy upon binding to PKR. Figure 2 shows that the emission anisotropy of mant-AMPPNP exhibits a large increase from ~0.02 to ~0.17 upon addition of a large excess of PKR.

Equilibrium Binding of ATP to PKR. On the basis of the large anisotropy changes upon binding of mant-nucleotides to PKR, we have chosen to use this method for detailed characterization of equilibrium binding parameters. Binding constants can reliably be obtained from anisotropy titrations performed using either variable enzyme or ligand concentrations. Figure 2 shows a titration of a fixed concentration of mant-AMPPNP with increasing concentrations of unphosphorylated, WT PKR; we refer to this format as a "forward titration". In contrast to previous reports (*13*, *14*), we find that ATP analogues bind readily to unactivated PKR.

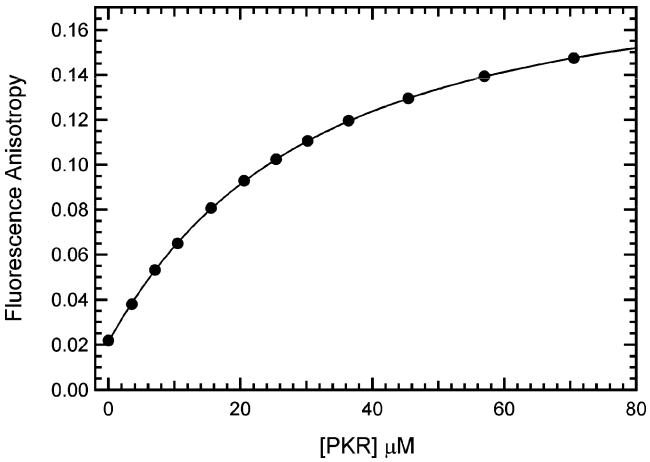

FIGURE 2: Binding of mant-AMPPNP to PKR measured by forward anisotropy titration. The fluorescence anisotropy of 20 μM mant-AMPPNP was measured at increasing concentrations of PKR at an excitation wavelength of 360 nm and an emission wavelength of 443 nm with spectral bandwidths of 2 and 4 nm for excitation and emission, respectively. The fluorescence intensity at each polarizer orientation was integrated for 1 s, and measurements were averaged until the maximum standard deviation drops below 0.1%. Each data point represents the average of three to four measurements. The solid line represents a fit of the data to a 1:1 binding model to obtain the following: $K_d = 33.8 \pm 0.7$ μM, $r_L = 0.0213 \pm 0.0003$, and $r_{EL} = 0.1914 \pm 0.0010$.

Analysis of the binding isotherm using eq 2 yields a K_d of 33.8 ± 0.7 μM, assuming a 1:1 binding stoichiometry (Table 1). If the stoichiometry is treated as an adjustable parameter, a best-fit value of 0.95 binding site/PKR monomer is obtained with a similar K_d of 31.3 μM. Thus, binding of mant-AMPPNP occurs with the expected 1:1 stoichiometry, indicating that our PKR preparations are fully competent for nucleotide binding. In subsequent analyses, the stoichiometries were fixed at 1:1 to improve the precision of the K_d determinations.

Although PKR exists in a monomer−dimer equilibrium (*29*), at the maximum enzyme concentration employed in the titration in Figure 2 only ~20% dimer is present. However, to prevent potential complications associated with variable extents of PKR dimerization during the course of a titration, we have devised an alternative reverse anisotropy titration in which the enzyme concentration is fixed and the ligand concentration is varied. Figure 3 shows a "reverse titration" using the same enzyme and ligand combination employed in Figure 2. The average anisotropy, $\langle r \rangle$, decreases with an increasing mant-AMPPNP concentration due to dilution of the bound ligand with excess free ligand, and the shape of this curve is determined by the dissociation constant. The reverse titration data were fit to a simple 1:1 binding isotherm using eq 2, giving a K_d value of 34.8 ± 3.6 μM, which closely agrees with the value obtained from the forward titration.

The reverse anisotropy titration assay was used to compare the K_d values for binding of mant-AMPPNP and mant-ATP to different PKR forms. Table 1 shows that the dissociation constant for binding of mant-AMPPNP to *in vitro*-phosphorylated PKR is, within error, no different from that of the unactivated enzyme. The K_d for a complex of unphosphorylated PKR with an activating 40 bp dsRNA is increased ~3-fold relative to that of the WT enzyme. Thus, there appears to be no strong correlation between activation of

Table 1: Equilibrium Dissociation Constants for Interaction of Nucleotides with PKR[a]

nucleotide	unphosphorylated	phosphorylated	K296R mutant	unphosphorylated with 40-mer dsRNA
mant-AMPPNP	33.8 ± 0.7 [b] 34.8 ± 3.6 [c]	34.0 ± 0.7 [b]	11.5 ± 0.3 [b]	102.3 ± 3.6 [c]
mant-ATP	–	24.6 ± 1.7[c]	10.3 ± 0.8 [b]	–
ATP	–	24.4 ± 0.1 [d]	20.2 ± 1.7 [d]	–
AMPPNP	97.7 ± 1.7 [d]	34.0 ± 0.1 [d]	22.8 ± 2.0 [d]	160.5 ± 1.4 [d]
ADP	76.5 ± 1.1 [d]	11.6 ± 0.7 [d]	12.5 ± 0.3 [d]	67.0 ± 0.7 [d]

[a] K_d values in units of micromolar. [b] Forward anisotropy titration. [c] Reverse anisotropy titration. [d] Competition titration using mant-AMPPNP.

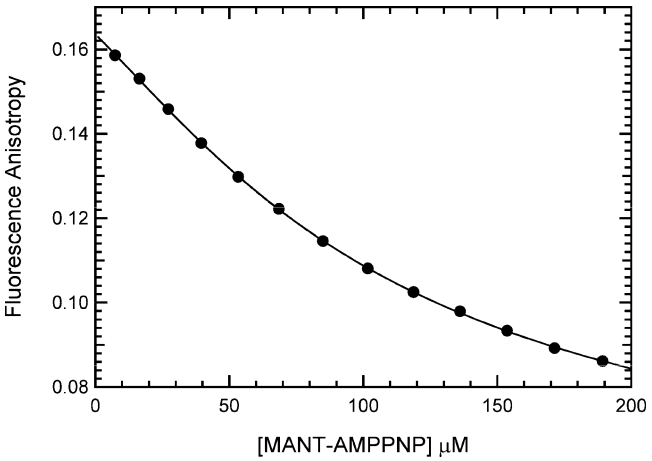

FIGURE 3: Binding of mant-AMPPNP to PKR measured by reverse fluorescence anisotropy. Mant-AMPPNP was titrated against 40 μM PKR, and the fluorescence anisotropy was measured at an excitation wavelength of 360 nm and an emission wavelength of 443 nm with spectral bandwidths of 2 and 4 nm for excitation and emission, respectively. Fluorescence intensities at each polarizer orientation were integrated for 1 s, and measurements were averaged until the maximum standard deviation drops below 0.1%. Each data point represents the average of three to four measurements. The solid line represents a fit of the data to a 1:1 binding model to obtain the following: $K_d = 34.8 \pm 3.6$ μM, $r_L = 0.0407 \pm 0.0016$, and $r_{EL} = 0.2356 \pm 0.0096$.

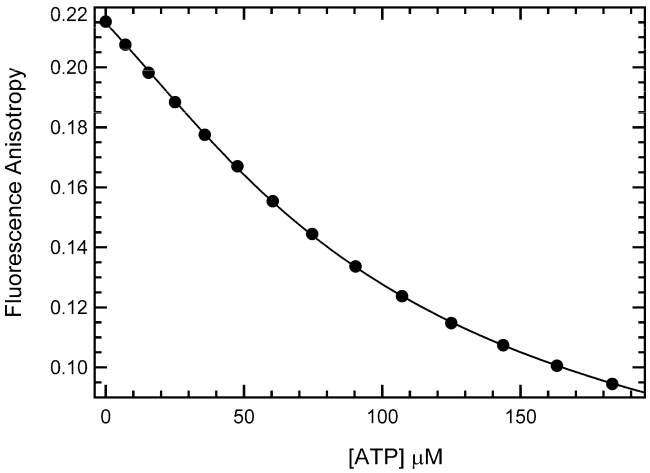

FIGURE 4: Binding of ATP to phosphorylated PKR measured by competition fluorescence anisotropy. In this case, ATP was titrated against 39.5 μM phosphorylated PKR (measured by UV absorption at 280 nm) with 11.3 μM mant-ATP and the fluorescence anisotropy measured with excitation and emission at 360 and 443 nm, respectively. Each data point represents an average of three to four repeated measurements. The K_d of binding of mant-ATP to phosphorylated PKR measured by reverse anisotropy titration and used in the fitting function was 24.6 μM.

PKR and enhanced nucleotide binding affinity; indeed, dsRNA binding slightly weakens nucleotide binding. Because PKR undergoes dsRNA-independent autophosphorylation at the higher protein concentrations used in the fluorescence measurements (*29*), it is not possible to directly characterize binding of mant-ATP to the WT, unphosphorylated enzyme without complications from the catalytic reaction. Thus, we have employed a catalytically inactive K296R mutant. In protein kinases, this lysine binds the α- and β-phosphates of ATP and is required for phosphoryl transfer but not ATP binding (*41*, *42*). Mant-AMPPNP binds to the K296R mutant with a K_d of 11.5 ± 0.3 μM, and a similar dissociation constant is observed for mant-ATP. For the phosphorylated enzyme, mant-ATP binds slightly stronger than mant-AMPPNP. Thus, the substitution of the $\beta-\gamma$ bridging O with N does not substantially affect ATP binding.

Competitive anisotropy titrations were performed to measure the binding affinity of unlabeled nucleotides. Figure 4 shows that unlabeled ATP effectively competes with mant-ATP for binding to phosphorylated PKR. Fitting the titration using the previously measured K_d for the labeled nucleotide gives a K_d of 24.4 ± 0.1 μM for unlabeled ATP; thus, the mant moiety does not perturb equilibrium binding of ATP to phosphorylated PKR. Similarly, mant does not alter the affinity of binding of AMPPNP to phosphorylated PKR (Table 1). However, mant enhances the affinity of binding of AMPPNP to WT, K296R, and the PKR−dsRNA complex by 3-, 2-, and ~1.5-fold, respectively. Finally, competition titrations were used to assess binding of the reaction product ADP. ADP binds ~2-fold more strongly than ATP to the phosphorylated and K296R enzymes and ~2-fold more strongly than AMPPNP to the PKR−dsRNA complex. However, the affinities of ADP and AMPPNP are approximately equal for unphosphorylated PKR.

Kinetics of Binding of Nucleotide to PKR. We have characterized the kinetics of binding of nucleotide to PKR by stopped-flow fluorescence measurements to define the binding mechanism and to determine whether the association or dissociation rates are sensitive to the enzyme activation state. Under pseudo-first-order conditions where the ligand is in excess, the most sensitive kinetic measurements are obtained by monitoring mant emission stimulated by tryptophan → mant energy transfer. Figure 5A shows that binding of 50 μM mant-ATP to unphosphorylated PKR gives rise to a large rapid fluorescence increase complete within 20 ms along with a slow, low-amplitude increase. The data fit well to a two-exponential model with a $k_{obs,1}$ of 514 ± 9 s^{-1} (96% amplitude) and a $k_{obs,2}$ of 39 ± 9 s^{-1} (4% amplitude). The fluorescence amplitude of the kinetic transient extrapolated to time zero corresponds to the fluorescence of the free ligand, indicating that there are no undetected fast phases within the instrument dead time (data not shown).

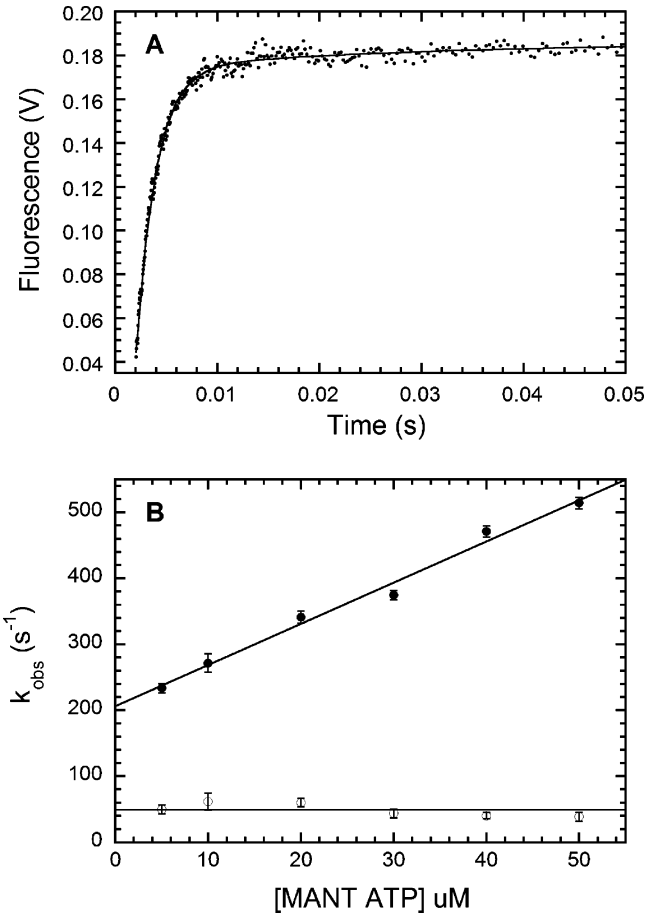

FIGURE 5: Kinetics of binding of mant-ATP to unphosphorylated WT PKR measured by stopped-flow fluorescence spectroscopy. (A) Time-dependent changes in fluorescence of 50 μM mant-ATP in the presence of 1 μM unphosphorylated PKR. The mixture was excited at 295 nm and the fluorescence emission above 400 nm was measured using a cutoff filter. The plot represents an average of 12 runs with each run made of 1000 data points taken over 10 s in a log time interval. The solid line is a two-exponential fit to the data. The first phase contributed 96% to the total amplitude with the observed rate constant ($k_{obs,1}$) of 514 $\pm$ 9 s^{-1}, while the second phase contributed 4% to the total amplitude with a $k_{obs,2}$ of 39 $\pm$ 9 s^{-1}. (B) Effect of mant-ATP concentration on k_{obs}. The solid line is a linear fit to the data from two experiments. $k_{obs,1}$ (●) increases linearly with the concentration of mant-ATP, and a least-squares fit yields a $k_{obs,1}$(slope) of 6.25 $\pm$ 0.35 μM^{-1} s^{-1} and a $k_{obs,1}$(intercept) of 206 $\pm$ 11 s^{-1}. $k_{obs,2}$ (○) is essentially independent of mant-ATP concentration with an average value of 48.9 $\pm$ 9.9 s^{-1}.

Figure 5B shows that the rate of the fast phase increases linearly with ligand concentration but the rate of the slow phase is essentially concentration-independent. The slope and intercept values for $k_{obs,1}$ and the average value of $k_{obs,2}$ are listed in Table 2. The relative amplitudes of the two phases are dependent on mant-ATP concentration: the contribution of $k_{obs,1}$ ranges from 87% at 5 μM ligand to 96% at 50 μM ligand (see Table S1 of the Supporting Information).

Because preparations of mant-ATP contain a mixture of 2′- and 3′-isomers, we also examined the binding kinetics of a single isomer nucleotide, 3′-mant-2′-deoxy-ATP. As with mant-ATP, 3′-mant-2′-deoxy-ATP binds to both WT and K296R PKR with biphasic association kinetics, indicating that this reaction pattern is not due to ligand heterogeneity (data not shown).

Binding of mant-ATP to other PKR forms also gives rise to a biexponential fluorescence increase with a concentration-dependent fast phase and a concentration-independent slow phase. Table 2 compares the kinetic parameters. Overall, the binding kinetics are not strongly affected by phosphorylation, binding to dsRNA, or the K296R mutation. The largest change occurs for K296R in which the value of the $k_{obs,1}$ intercept is decreased ~2-fold relative to that of unphosphorylated PKR. Also, in all cases, the relative amplitude of the fast phase increases with an increase in ligand concentration (see Table S1 of the Supporting Information). For the phosphorylated and dsRNA-bound forms, the relative amplitudes are similar to the unphosphorylated enzyme; however, for the K296R mutant, the fraction of the fast phase varies more strongly, increasing from 44 to 91% between 10 and 50 μM mant-AMPPNP.

The dissociation kinetics for mant-ATP were directly measured by trapping experiments in which the PKR−mant-ATP complex was mixed with a large molar excess of unlabeled ATP. Figure 6 shows that the dissociation of mant-ATP from unphosphorylated PKR occurs with a dominant fast phase with a $k_{obs,1}$ of 175 $\pm$ 2 s^{-1} (94% amplitude) and a slow, low-amplitude phase with a $k_{obs,2}$ of 43.1 $\pm$ 5.5 s^{-1}. Biphasic dissociation kinetics were observed for the other PKR forms (Table 2). As in the case of the association kinetics, the observed rate constants for dissociation are fairly similar for the different PKR forms. The most notable effect is a decrease in both $k_{obs,1}$ and $k_{obs,2}$ for the K296R mutant. More dramatic changes are observed in the relative amplitudes of the two phases: for phosphorylated PKR, the fast phase decreases to 49%, and for the K296R mutant, it drops to 13%.

The presence of two rate constants for the binding of mant-ATP indicates a minimal two-step kinetic mechanism involving bimolecular association and isomerization reactions. In Scheme 1, the nucleotide first binds to PKR to form EL, which then undergoes a conformational change to E′L.

Table 2: Kinetics of Binding of Mant-ATP to PKR

	association kinetics			dissociation kinetics[a]	
enzyme form	$k_{obs,1}$(slope) (μM^{-1} s^{-1})[b]	$k_{obs,1}$(intercept) (s^{-1})[c]	$k_{obs,2}$(average) (s^{-1})[d]	$k_{obs,1}$ (s^{-1})	$k_{obs,2}$ (s^{-1})
unphosphorylated	6.25 $\pm$ 0.35	206 $\pm$ 11	48.9 $\pm$ 9.9	175 $\pm$ 2	43.1 $\pm$ 5.5
phosphorylated	4.75 $\pm$ 0.40	239 $\pm$ 14	43.2 $\pm$ 4.9	214 $\pm$ 5	56.0 $\pm$ 0.8
K296R	5.56 $\pm$ 0.38	91 $\pm$ 13	39.7 $\pm$ 5.7	134 $\pm$ 4	18.6 $\pm$ 0.1
unphosphorylated + 40-mer dsRNA	5.36 $\pm$ 0.50	232 $\pm$ 16	36.5 $\pm$ 8.1	175 $\pm$ 1	23.2 $\pm$ 5.5

[a] Dissociation kinetics measured upon addition of 2 mM unlabeled ATP. [b] Slope from the linear fit of $k_{obs,1}$ vs mant-ATP concentration. [c] Y intercept from the linear fit of $k_{obs,1}$ vs mant-ATP concentration. [d] Average value of $k_{obs,2}$ over the entire range of mant-ATP concentrations.

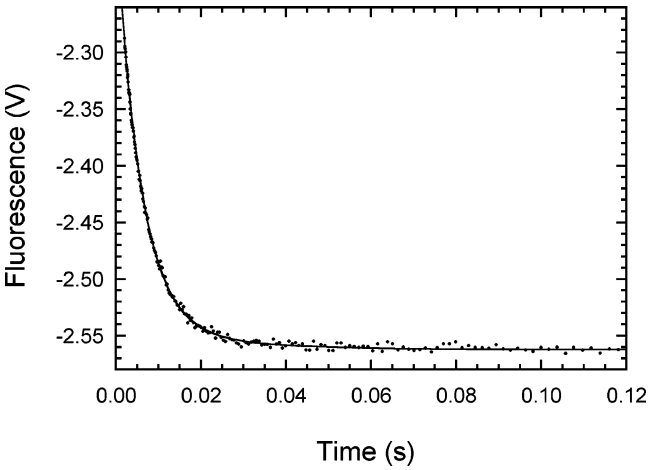

FIGURE 6: Kinetics of dissociation of mant-ATP from unphosphorylated WT PKR measured by stopped-flow fluorescence spectroscopy. Time-dependent changes in fluorescence of 40 μM mant-ATP in the presence of 1 μM unphosphorylated PKR were competed with 2 mM ATP. The mixture was excited at 295 nm and fluorescence emission above 400 nm measured using a cutoff filter. The plot represents an average of 21 runs with each run made of 1000 data points taken over 10 s in a log time interval. The solid line is the two-exponential fit to the data. The first phase contributed 94% to the total amplitude with a rate constant ($k_{obs,1}$) of 175 ± 2 s^{-1}, while the second phase contributed 6% to the total amplitude with a $k_{obs,2}$ of 43.1 ± 5.5 s^{-1}.

Scheme 1

$$E + L \underset{k_{-1}}{\overset{k_1}{\rightleftharpoons}} EL \underset{k_{-2}}{\overset{k_2}{\rightleftharpoons}} E'L$$

Scheme 2

$$E + L \underset{k_{-1}}{\overset{k_1}{\rightleftharpoons}} E' + L \underset{k_{-2}}{\overset{k_2}{\rightleftharpoons}} E'L$$

Alternatively, the free enzyme may undergo a conformational change (E $\rightarrow$ E′) prior to binding nucleotide (Scheme 2).

Although these two mechanisms cannot be distinguished solely on the basis of the measured rate constants (*43*), only Scheme 1 is fully consistent with the kinetic data. In Scheme 2, E′L is the only species that gives rise to fluorescence energy transfer, and in the dissociation experiments, its decay would be monoexponential with a rate constant of k_{-2}. However, a biexponential fluorescence decrease is observed experimentally (Figure 6). In contrast, Scheme 1 predicts biexponential decay kinetics for the dissociation experiment. For the association reaction, both schemes predict that formation of E′L proceeds with a lag phase associated with population of an intermediate (either EL or E′). However, no lag phase is observed, and both kinetic phases of the association reaction have positive amplitudes, indicating that Scheme 2 is incorrect. Scheme 1 is consistent with the data provided that both EL and E′L contribute to the fluorescence increase, giving rise to an overall fluorescence change with two positive kinetic phases.

For Scheme 1, the values of fast and slow phases can be expressed in terms of the elementary rate constants using the square root approximation (*43*) to give

$$k_{obs,1} = k_1[S] + k_{-1} + k_2 + k_{-2} \quad (5)$$

$$k_{obs,2} = \frac{k_1[S](k_{-2} + k_2) + k_{-1}k_{-2}}{k_1[S] + k_{-1} + k_2 + k_{-2}} \quad (6)$$

Thus, as observed in Figure 5B, $k_{obs,1}$ should exhibit a linear substrate concentration dependence, where the slope is given by k_1 and the intercept by $k_{-1} + k_2 + k_{-2}$. Although $k_{obs,2}$ is predicted to show a hyperbolic concentration dependence, this dependence may not be apparent in systems in which k_2 and k_{-2} are small compared to k_1[S] and k_{-1}. In the limit of a single-step mechanism, where the isomerization reaction is not present, $k_2 = k_{-2} = 0$ and only a single-exponential phase is expected for which $k_{obs} = k_1[S] + k_{-1}$. For the unphosphorylated enzyme, if we neglect the slow kinetic phase and calculate K_d ($=k_{-1}/k_1$) on the basis of the intercept and slope of $k_{obs,1}$, we obtain a K_d value of 33.0 μM, which agrees well with the K_d equilibrium values of 34−35 μM for mant-AMPPNP (Table 1). This agreement presumably is associated with the small contribution of the slow phase and small population of the E′L state for this enzyme form.

Figure 7 shows a global fit of the WT PKR binding kinetics to Scheme 1 over the concentration range of 5−30 μM mant-ATP, making the simplifying assumption that EL and E′L contribute equally to the observed fluorescence change. The good fit provides further support for Scheme 1 and gives the following best values: $k_1 = 7.33 \pm 0.07$ μM^{-1} s^{-1}, $k_{-1} = 137 \pm 2$ s^{-1}, $k_2 = 1.8 \pm 0.7$ s^{-1}, and $k_{-2} = 13.0 \pm 10.7$ s^{-1}. The parameters obtained from the global analysis are reasonably consistent with the value of k_1 obtained from the linear substrate concentration dependence of $k_{obs,1}$ and with the trapping experiments, where the fast phase is equal to k_{-1} and the slow phase corresponds to k_{-2}. Although the standard errors for k_2 and k_{-2} are large, it is clear that ligand binding and dissociation are significantly faster than the subsequent isomerization reaction.

Atomic Force Microscopy. In AFM images of latent PKR (Figure 8A), we observe molecules with clearly resolved features. On the basis of volume analysis of the individual particles, we identify the molecules as monomers of the protein (data not shown). A large number of proteins have been imaged using AFM in air on mica surfaces (*40*, *44*−*49*). In these images, proteins generally appear globular with little or no disordered regions, although multiple domains and multiple subunits have been resolved in a few cases (D. A. Erie, unpublished data; *45*, *50*). The degree of structure apparent in the images of the PKR monomers is striking for a small (62 kDa) protein.

The AFM images the PKR monomers reveal up to three distinguishable structured regions linked by bridgelike stretches. In some cases, the linker regions are structured (for example, Figure 8B, panel 4); however, this structured conformation appears to be unstable because in most molecules the linker adopts an unfolded, extended form. We have classified the different observed conformations into four groups, as shown in Figure 8B. Some molecules feature a compact arrangement (Figure 8B, panel 4), while others appear almost completely extended (Figure 8B, panel 1). Statistical analysis of the different conformations shows that the four shape categories are represented with approximately equal frequencies in the images (data not shown), which is consistent with a high linker flexibility.

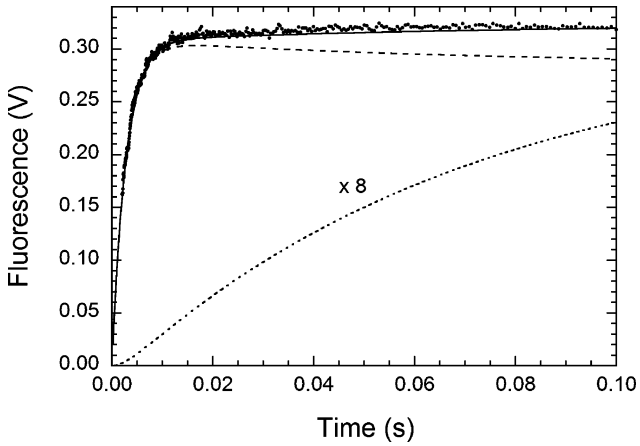

FIGURE 7: Simulation of the kinetics of mant-ATP binding to unphosphorylated PKR: [EL] (- - -), [E′L] × 8 (•••), and [EL] + [E′L] (—). The kinetics were simulated on the basis of a global fit of the experimental data to Scheme 1 over the range of 5−30 μM mant-ATP, assuming that EL and E′L contribute equally. The adjustable parameters are the four rate constants and an overall scaling factor, giving the following best fit values: $k_1 = 7.33 \pm 0.07\ \mu M^{-1}\ s^{-1}$, $k_{-1} = 137 \pm 2\ s^{-1}$, $k_2 = 1.8 \pm 0.7\ s^{-1}$, and $k_{-2} = 13.0 \pm 10.7\ s^{-1}$.

Addition of ATP had no effect on the molecular conformations of PKR seen in AFM (data not shown). Because these experiments were carried out at low protein concentrations, PKR did not undergo dsRNA autophosphorylation during AFM analysis (*29*). Phosphorylated PKR (Figure 8C) exhibited volumes consistent with PKR monomers and dimers (and higher oligomeric states), in agreement with previous studies finding enhanced dimerization of phosphorylated PKR (*29*). Although the phosphorylated protein frequently exhibited globular, condensed shapes, many of the molecules still displayed open extended shapes similar to those seen for unphosphorylated PKR, suggesting that the kinase domain is accessible to substrate in both the unphosphorylated protein and the phosphorylated protein.

DISCUSSION

A key finding from our equilibrium and kinetic studies of nucleotide binding to PKR is that ATP is capable of binding to the unphosphorylated enzyme, and the dissociation constants and kinetics are largely unaffected by phosphorylation or binding to dsRNA. Although slight changes in PKR affinity and binding kinetics are observed, these differences are not likely to be physiologically significant, since the millimolar intracellular concentration of ATP is ~2 orders of magnitude higher than the average K_d. These results contrast with earlier studies indicating that photo-cross-linking of either ATP or 8-azido ATP to PKR requires dsRNA (*13*, *14*) or prior autophosphorylation (*14*). The origin of these discrepancies is not clear but may be related to differences in methodology or sample preparation. In particular, the current measurements were performed using direct fluorescence binding methods with purified enzyme. Control experiments demonstrate that the mant fluorophore does not strongly perturb the affinity or kinetics.

On the basis of the nucleotide binding data, we cannot exclude the possibility that dsRNA binding or phosphorylation alters the accessibility of the peptide substrate binding region. No correlation between substrate recognition and dsRNA binding has been described. However, it has been reported that binding of eIF2α to a PKR kinase domain construct requires phosphorylation at threonine 446 within the activation loop, whereas K_m for the nonspecific substrate histone H2A is unaffected by PKR phosphorylation (*34*). In contrast, earlier studies using full-length PKR demonstrated that eIF2α can bind to unphosphorylated PKR (*51*). Although the activities of many eukaryotic protein kinases are enhanced by phosphorylation events within the activation loop, in most cases, peptide substrate or nucleotide binding is not controlled by phosphorylation; instead, the dominant effect is to enhance the phosphoryl transfer rate (*33*, *52*). Further studies are required to determine whether PKR follows this dominant paradigm.

Although mutation of lysine 296 renders PKR completely inactive (*53*), the K296R mutant is capable of binding adenosine nucleotides. This lysine is conserved in most kinases where it interacts with the α- and β-phosphates of ATP. Mutants of this lysine in other kinases, including lck (*42*), erk2 (*41*), and PKA (*54*), are also capable of binding ATP but are catalytically impaired. In PKR, the K296R mutation decreases adenosine nucleotide K_d values by 3−6-fold, but in erk2, the analogous lysine → arginine mutation slightly increases the K_m for ATP, suggesting that the lysine−ATP interaction does not contribute strongly to the overall binding affinity.

The observation of biphasic kinetics in the stopped-flow measurements of binding of ATP to PKR supports a minimal two-step model involving bimolecular association and isomerization steps. In general, these steps can occur in either order; however, only Scheme 1, in which binding precedes the isomerization reaction, is consistent with the biphasic fluorescence decrease observed in dissociation experiments and the presence of two positive phases in the association measurements. Furthermore, kinetic transients obtained at multiple ligand concentrations can be globally fit to Scheme 1. Qualitatively similar kinetics are observed in all PKR forms, indicating that the overall reaction mechanism is not altered by phosphorylation, dsRNA binding, or the K296R mutation. Transient kinetic measurements have led to a similar kinetic model for binding of nucleotide to protein kinase A involving ligand binding and subsequent isomerization; however, an additional kinetic phase was observed and assigned to an additional isomerization step (*35*). On the basis of kinetic data alone, the isomerization step cannot be definitively assigned to a specific conformational change or to a step in the catalytic cycle. The ATP-bound form of the PKR kinase domain has a slightly more open conformation of the two lobes of the catalytic core than the unliganded kinase (*8*), suggesting that PKR undergoes a conformational change upon nucleotide binding. The slow isomerization may be associated with this conformational change.

The AFM images of latent PKR reveal monomeric molecules that are extended and segmented. These highly asymmetric structures are fully consistent with the previously reported high frictional ratio, f/f_0, of 1.62 (*29*) and the large radius of gyration for PKR (*19*). Structured domains are resolved in the AFM images and are linked by flexible, bridge-like regions. Resolution of this domain structure indicates that latent PKR exists in an open conformation consistent with unhindered binding of ATP to the kinase domain. The range of different PKR conformations observed

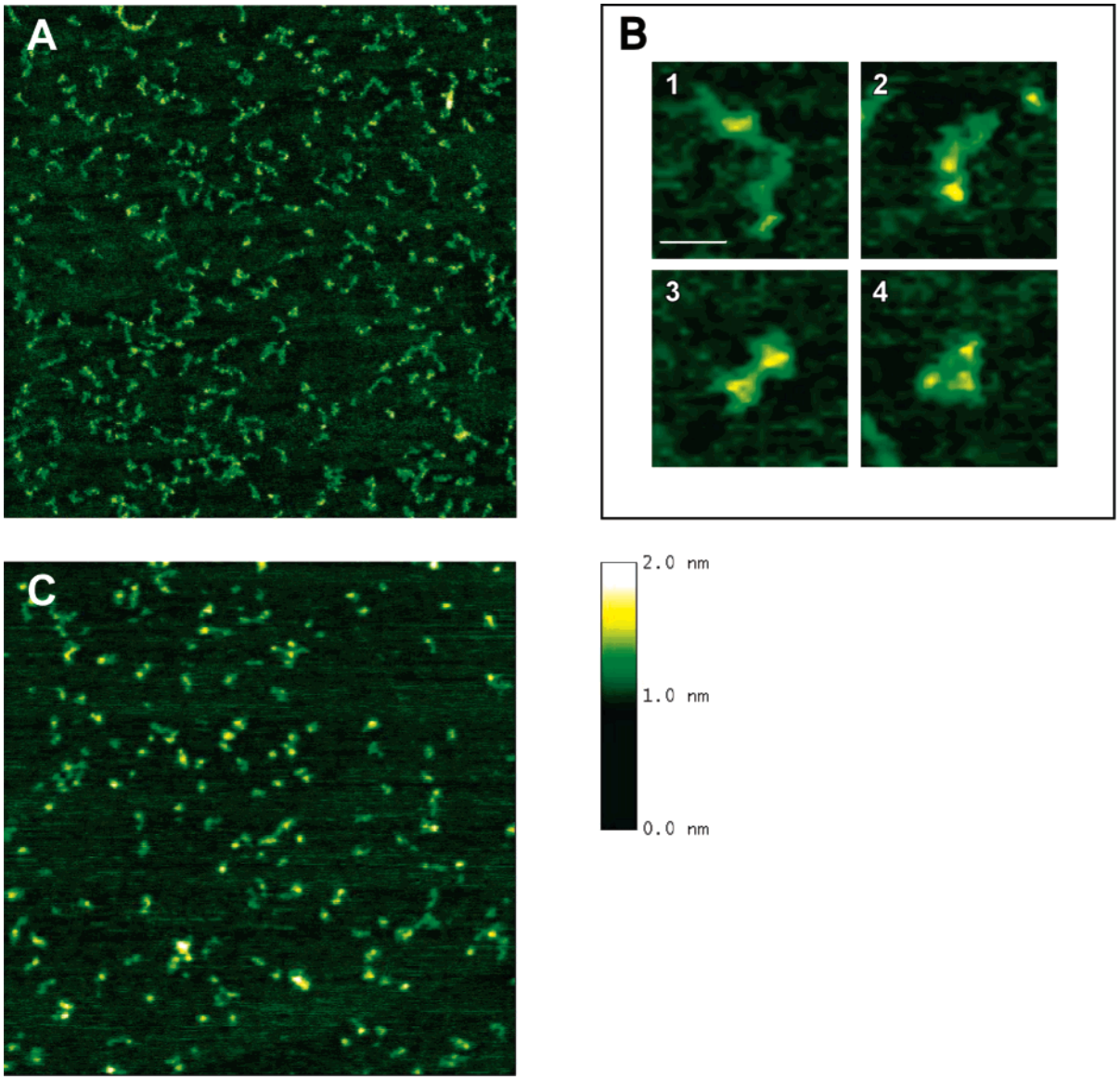

FIGURE 8: AFM images of (A) unphosphorylated PKR and (C) phosphorylated PKR. Images are 1 μm × 1 μm with a height scale of 2 nm. In panel A, different molecular conformations can be found. Examples of these are shown enlarged in panel B: almost entirely extended conformation (1), shapes with three resolvable segments (2), shapes showing only two resolved segments and a broader linking region (3), and molecules in which the individual segments are very close together (4). The scale bar in panel 1 is 20 nm. The height scale of all images is 2 nm as indicated next to panel C.

on a surface using AFM indicates that highly flexible regions link the individual segments, allowing these domains to land on the surface in different orientations and at different distances from each other. In some cases, the linker regions appear to be structured; however, this structured conformation is very unstable since the majority of these regions adopt an unfolded, extended conformation. The high flexibility of these regions is consistent with NMR evidence that the 20-amino acid linker between the dsRBMs is unstructured in solution (*7*). The conformation of the ~100-residue segment lying between the dsRBD and kinase domain is unknown but may contain additional flexible regions. Although globular, condensed shapes are frequently observed in the AFM images of phosphorylated PKR, many molecules exhibit domain structure. Thus, phosphorylated PKR can adopt an open shape similar to that of the latent enzyme, consistent with an insignificant effect of the protein phosphorylation state on ATP binding affinity.

Our nucleotide binding and AFM data do not support the autoinhibition model for PKR activation and indicate an open conformation for the resting enzyme. Equilibrium and kinetic measurements of nucleotide binding demonstrate that the ATP binding site is fully accessible in the unphosphorylated enzyme in the absence of dsRNA. AFM data indicate that the dsRBD is not stably associated with the kinase domain. PKR can be activated by dimerization at high protein concentrations in the absence of dsRNA (*29*), arguing against a specific involvement of the dsRNA binding domains in enzymatic activation. In addition, fusion of a heterologous dimerization domain with the PKR catalytic domain enhances autophosphorylation and eIF2α kinase function *in vivo*, suggesting that dimerization is sufficient to induce activation in the absence of an exogenous activator (*9*). Heparin, a known activator, is capable of activating PKR deletion mutants lacking the dsRNA binding domain (*55*, *56*), providing further evidence that the dsRNA binding domain

is not directly associated with enzymatic activity. Thus, PKR activation by dsRNA and heparin may simply be associated with an increase in the local enzyme concentration and enhancement of functional dimerization by binding PKR to a polymeric substrate containing multiple binding sites.

ACKNOWLEDGMENT

We thank Carolyn Teschke for use of the fluorescence stopped-flow instrument, Eric Anderson for help in carrying out the kinetic measurements, and Ray Brown for modeling of mant-ATP into the PKR kinase active site.

SUPPORTING INFORMATION AVAILABLE

Relative contribution of the fast phase for association of mant-AMPNP with PKR (Table S1). This material is available free of charge via the Internet at http://pubs.acs.org.

REFERENCES

1. Clemens, M. J. (1997) PKR: A protein kinase regulated by double-stranded RNA, *Int. J. Biochem. Cell Biol. 29*, 945−949.
2. Stark, G. R., Kerr, I. M., Williams, B. R., Silverman, R. H., and Schreiber, R. D. (1998) How cells respond to interferons, *Annu. Rev. Biochem. 67*, 227−264.
3. Williams, B. R. (2001) Signal integration via PKR, *Sci. STKE 2001*, RE2.
4. Dever, T. E. (2002) Gene-specific regulation by general translation factors, *Cell 108*, 545−556.
5. Barber, G. N. (2001) Host defense, viruses and apoptosis, *Cell Death Differ. 8*, 113−126.
6. Tian, B., Bevilacqua, P. C., Diegelman-Parente, A., and Mathews, M. B. (2004) The double-stranded RNA binding motif: Interference and much more, *Nat. Rev. Mol. Cell Biol. 5*, 1013−1023.
7. Nanduri, S., Carpick, B. W., Yang, Y., Williams, B. R., and Qin, J. (1998) Structure of the double-stranded RNA binding domain of the protein kinase PKR reveals the molecular basis of its dsRNA-mediated activation, *EMBO J. 17*, 5458−5465.
8. Dar, A. C., Dever, T. E., and Sicheri, F. (2005) Higher-order substrate recognition of eIF2α by the RNA-dependent protein kinase PKR, *Cell 122*, 887−900.
9. Vattem, K. M., Staschke, K. A., and Wek, R. C. (2001) Mechanism of activation of the double-stranded-RNA-dependent protein kinase, PKR: Role of dimerization and cellular localization in the stimulation of PKR phosphorylation of eukaryotic initiation factor-2 (eIF2), *Eur. J. Biochem. 268*, 3674−3684.
10. Nanduri, S., Rahman, F., Williams, B. R. G., and Qin, J. (2000) A dynamically tuned double-stranded RNA binding mechanism for the activation of antiviral kinase PKR, *EMBO J. 19*, 5567−5574.
11. Wu, S., and Kaufman, R. J. (2004) trans-Autophosphorylation by the isolated kinase domain is not sufficient for dimerization or activation of the dsRNA-activated protein kinase PKR, *Biochemistry 43*, 11027−11034.
12. Wu, S., and Kaufman, R. J. (1997) A model for the double-stranded RNA (dsRNA)-dependent dimerization and activation of the dsRNA-activated protein kinase PKR, *J. Biol. Chem. 272*, 1291−1296.
13. Bischoff, J. R., and Samuel, C. E. (1985) Mechanism of interferon action. The interferon-induced phosphoprotein P1 possesses a double-stranded RNA-dependent ATP-binding site, *J. Biol. Chem. 260*, 8237−8239.
14. Galabru, J., and Hovanessian, A. (1987) Autophosphorylation of the protein kinase dependent on double-stranded RNA, *J. Biol. Chem. 262*, 15538−15544.
15. Rivas, C., Gil, J., and Esteban, M. (1999) Identification of functional domains of the interferon-induced enzyme PKR in cells lacking endogenous PKR, *J. Interferon Cytokine Res. 19*, 1229−1236.
16. Vattem, K. M., Staschke, K. A., Zhu, S., and Wek, R. C. (2001) Inhibitory sequences in the N-terminus of the double-stranded-RNA-dependent protein kinase, PKR, are important for regulating phosphorylation of eukaryotic initiation factor 2α (eIF2α), *Eur. J. Biochem. 268*, 1143−1153.
17. Saelens, X., Kalai, M., and Vandenabeele, P. (2001) Translation inhibition in apoptosis: Caspase-dependent PKR activation and eIF2-α phosphorylation, *J. Biol. Chem. 276*, 41620−41628.
18. Zhu, S., Romano, P. R., and Wek, R. C. (1997) Ribosome targeting of PKR is mediated by two double-stranded RNA-binding domains and facilitates in vivo phosphorylation of eukaryotic initiation factor-2, *J. Biol. Chem. 272*, 14434−14441.
19. Carpick, B. W., Graziano, V., Schneider, D., Maitra, R. K., Lee, X., and Williams, B. R. G. (1997) Characterization of the solution complex between the interferon-induced double-stranded RNA-activated protein kinase and HIV-1 trans-activating region RNA, *J. Biol. Chem. 272*, 9510−9516.
20. Manche, L., Green, S. R., Schmedt, C., and Mathews, M. B. (1992) Interactions between double-stranded RNA regulators and the protein kinase DAI, *Mol. Cell. Biol. 12*, 5238−5248.
21. Kostura, M., and Mathews, M. B. (1989) Purification and activation of the double-stranded RNA-dependent eIF-2 kinase DAI, *Mol. Cell. Biol. 9*, 1576−1586.
22. Taylor, D. R., Lee, S. B., Romano, P. R., Marshak, D. R., Hinnebusch, A. G., Esteban, M., and Mathews, M. B. (1996) Autophosphorylation sites participate in the activation of the double-stranded-RNA-activated protein kinase PKR, *Mol. Cell. Biol. 16*, 6295−6302.
23. Taylor, D. R., Tian, B., Romano, P. R., Hinnebusch, A. G., Lai, M. M., and Mathews, M. B. (2001) Hepatitis C virus envelope protein E2 does not inhibit PKR by simple competition with autophosphorylation sites in the RNA-binding domain, *J. Virol. 75*, 1265−1273.
24. Romano, P. R., Garcia-Barrio, M. T., Zhang, X., Wang, Q., Taylor, D. R., Zhang, F., Herring, C., Mathews, M. B., Qin, J., and Hinnebusch, A. G. (1998) Autophosphorylation in the activation loop is required for full kinase activity in vivo of human and yeast eukaryotic initiation factor 2α kinases PKR and GCN2, *Mol. Cell. Biol. 18*, 2282−2297.
25. Zhang, F., Romano, P. R., Nagamura-Inoue, T., Tian, B., Dever, T. E., Mathews, M. B., Ozato, K., and Hinnebusch, A. G. (2001) Binding of double-stranded RNA to protein kinase PKR is required for dimerization and promotes critical autophosphorylation events in the activation loop, *J. Biol. Chem. 276*, 24946−24958.
26. Zhang, X., Herring, C. J., Romano, P. R., Szczepanowska, J., Brzeska, H., Hinnebusch, A. G., and Qin, J. (1998) Identification of phosphorylation sites in proteins separated by polyacrylamide gel electrophoresis, *Anal. Chem. 70*, 2050−2059.
27. Su, Q., Wang, S., Baltzis, D., Qu, L. K., Wong, A. H., and Koromilas, A. E. (2006) Tyrosine phosphorylation acts as a molecular switch to full-scale activation of the eIF2{α} RNA-dependent protein kinase, *Proc. Natl. Acad. Sci. U.S.A. 103*, 63−68.
28. Galabru, J., Katze, M. G., Robert, N., and Hovanessian, A. G. (1989) The binding of double-stranded RNA and adenovirus VAI RNA to the interferon-induced protein kinase, *Eur. J. Biochem. 178*, 581−589.
29. Lemaire, P. A., Lary, J., and Cole, J. L. (2005) Mechanism of PKR activation: Dimerization and kinase activation in the absence of double-stranded RNA, *J. Mol. Biol. 345*, 81−90.
30. Nolen, B., Taylor, S., and Ghosh, G. (2004) Regulation of protein kinases: Controlling activity through activation segment conformation, *Mol. Cell 15*, 661−675.
31. Johnson, L. N., Noble, M. E. M., and Owen, D. J. (1996) Active and inactive protein kinases: Structural basis of regulation, *Cell 85*, 149−158.
32. Huse, M., and Kuriyan, J. (2002) The conformational plasticity of protein kinases, *Cell 109*, 275−282.
33. Adams, J. A. (2001) Kinetic and catalytic mechanisms of protein kinases, *Chem. Rev. 101*, 2271−2290.
34. Dey, M., Cao, C., Dar, A. C., Tamura, T., Ozato, K., Sicheri, F., and Dever, T. E. (2005) Mechanistic link between PKR dimerization, autophosphorylation, and eIF2α substrate recognition, *Cell 122*, 901−913.
35. Ni, Q., Shaffer, J., and Adams, J. A. (2000) Insights into nucleotide binding in protein kinase A using fluorescent adenosine derivatives, *Protein Sci. 9*, 1818−1827.
36. Talavera, M. A., and De La Cruz, E. M. (2005) Equilibrium and kinetic analysis of nucleotide binding to the DEAD-box RNA helicase DbpA, *Biochemistry 44*, 959−970.
37. Barshop, B. A., Wrenn, R. F., and Frieden, C. (1983) Analysis of numerical methods for computer simulation of kinetic processes: Development of KINSIM: A flexible, portable system, *Anal. Biochem. 130*, 134−145.

38. Anderson, K. S., Sikorski, J. A., and Johnson, K. A. (1988) A tetrahedral intermediate in the EPSP synthase reaction observed by rapid quench kinetics, *Biochemistry 27*, 7395−7406.
39. Yang, Y., Wang, H., and Erie, D. A. (2003) Quantitative characterization of biomolecular assemblies and interactions using atomic force microscopy, *Methods 29*, 175−187.
40. Ratcliff, G. C., and Erie, D. A. (2001) A novel single-molecule study to determine protein−protein association constants, *J. Am. Chem. Soc. 123*, 5632−5635.
41. Robinson, M. J., Harkins, P. C., Zhang, J., Baer, R., Haycock, J. W., Cobb, M. H., and Goldsmith, E. J. (1996) Mutation of position 52 in ERK2 creates a nonproductive binding mode for adenosine 5′-triphosphate, *Biochemistry 35*, 5641−5646.
42. Carrera, A. C., Alexandrov, K., and Roberts, T. M. (1993) The conserved lysine of the catalytic domain of protein kinases is actively involved in the phosphotransfer reaction and not required for anchoring ATP, *Proc. Natl. Acad. Sci. U.S.A. 90*, 442−446.
43. Johnson, K. A. (1992) Transient state kinetic analysis of enzyme reaction pathways, in *The Enzymes* (Sigman, D. S., Ed.) pp 1−61, Academic Press, San Diego.
44. Dame, R. T., Wyman, C., and Goosen, N. (2003) Insights into the regulation of transcription by scanning force microscopy, *J. Microsc. 212*, 244−253.
45. Janicijevic, A., Ristic, D., and Wyman, C. (2003) The molecular machines of DNA repair: Scanning force microscopy analysis of their architecture, *J. Microsc. 212*, 264−272.
46. Xue, Y., Ratcliff, G. C., Wang, H., Davis-Searles, P. R., Gray, M. D., Erie, D. A., and Redinbo, M. R. (2002) A minimal exonuclease domain of WRN forms a hexamer on DNA and possesses both 3′-5′ exonuclease and 5′-protruding strand endonuclease activities, *Biochemistry 41*, 2901−2912.
47. Thomson, N. H., Smith, B. L., Almqvist, N., Schmitt, L., Kashlev, M., Kool, E. T., and Hansma, P. K. (1999) Oriented, active *Escherichia coli* RNA polymerase: An atomic force microscope study, *Biophys. J. 76*, 1024−1033.
48. Kasas, S., Thomson, N. H., Smith, B. L., Hansma, H. G., Zhu, X., Guthold, M., Bustamante, C., Kool, E. T., Kashlev, M., and Hansma, P. K. (1997) *Escherichia coli* RNA polymerase activity observed using atomic force microscopy, *Biochemistry 36*, 461−468.
49. Wyman, C., Rombel, I., North, A. K., Bustamante, C., and Kustu, S. (1997) Unusual oligomerization required for activity of NtrC, a bacterial enhancer-binding protein, *Science 275*, 1658−1661.
50. Shiomi, Y., Usukura, J., Masamura, Y., Takeyasu, K., Nakayama, Y., Obuse, C., Yoshikawa, H., and Tsurimoto, T. (2000) ATP-dependent structural change of the eukaryotic clamp-loader protein, replication factor C, *Proc. Natl. Acad. Sci. U.S.A. 97*, 14127−14132.
51. Cai, R., and Williams, B. R. (1998) Mutations in the double-stranded RNA-activated protein kinase insert region that uncouple catalysis from eIF2α binding, *J. Biol. Chem. 273*, 11274−11280.
52. Adams, J. A. (2003) Activation loop phosphorylation and catalysis in protein kinases: Is there functional evidence for the autoinhibitor model? *Biochemistry 42*, 601−607.
53. Katze, M. G., Wambach, M., Wong, M. L., Garfinkel, M., Meurs, E., Chong, K., Williams, B. R., Hovanessian, A. G., and Barber, G. N. (1991) Functional expression and RNA binding analysis of the interferon-induced, double-stranded RNA-activated, 68,000-Mr protein kinase in a cell-free system, *Mol. Cell. Biol. 11*, 5497−5505.
54. Iyer, G. H., Garrod, S., Woods, V. L., Jr., and Taylor, S. S. (2005) Catalytic independent functions of a protein kinase as revealed by a kinase-dead mutant: Study of the Lys72His mutant of cAMP-dependent kinase, *J. Mol. Biol. 351*, 1110−1122.
55. Patel, R. C., Stanton, P., and Sen, G. C. (1994) Role of the amino-terminal residues of the interferon-induced protein kinase in its activation by double-stranded RNA and heparin, *J. Biol. Chem. 269*, 18593−18598.
56. Patel, R. C., and Sen, G. C. (1998) Requirement of PKR dimerization mediated by specific hydrophobic residues for its activation by double-stranded RNA and its antigrowth effects in yeast, *Mol. Cell. Biol. 18*, 7009−7019.

BI060567D